IMPACT OF ACTIVE AEROELASTIC WING TECHNOLOGY ON WING GEOMETRY USING RESPONSE SURFACE METHODOLOGY

P. Scott Zink*, Dimitri N. Mavris†
Georgia Institute of Technology, Atlanta, Georgia

Peter M. Flick‡
Wright-Patterson Air Force Base, Dayton, Ohio

Michael H. Love§
Lockheed Martin Tactical Aircraft Systems, Ft. Worth, Texas

Abstract

A multidisciplinary design study considering the impact of Active Aeroelastic Wing (AAW) technology on the wing geometry of a lightweight fighter concept is presented. The study incorporates multidisciplinary design optimization (MDO) and response surface methods to characterize wing weight as a function of wing geometry. The study involves the sizing of the wing box skins of several fighter configurations to minimum weight subject to maneuver requirements. In addition, the MDO problem makes use of a new capability, trim optimization for redundant control surfaces, to accurately model AAW technology. The response surface methodology incorporates design of experiments, least squares regression, and makes use of the parametric definition of a structural finite element model and aerodynamic model to build response surface equations of wing weight as a function of wing geometric parameters for both AAW technology and conventional control technology. The goal for this design study is to demonstrate a process by which some of the benefits associated with AAW technology can be quantified over the wing geometry design space, so that future conceptual designers may make the best use of AAW technology.

Introduction

Conventional aircraft design philosophy views the aeroelastic deformation of an aircraft wing as having a negative impact on aerodynamic and control system performance. The twisting of a wing due to aileron deflection during a roll maneuver can produce the phenomena of aileron reversal. Aileron reversal is the point where the deflection of the aileron produces no rolling moment[1]. That is, the rolling moment produced by the change in camber due to aileron deflection is offset by the reduction in effective wing angle of attack due to aeroelastic wing twist. Aircraft designers have generally tried to limit the effects of aeroelastic deformation by designing geometrically stiff planforms (low aspect ratio, high t/c), increasing structural weight to provide additional stiffness, and/or using horizontal tails to provide supplemental roll moment. A conventional wing design presents a severe compromise between aerodynamic, control, and structural performance.

An emerging and promising technology for addressing the problem of adverse aeroelastic deformation is Active Aeroelastic Wing (AAW) technology. It has recently been a key area of study for both the government and industry[2,3] and is defined by Pendleton et. al., as "a multidisciplinary, synergistic technology that integrates air vehicle aerodynamics, active controls, and structures together to maximize air vehicle performance"[4]. AAW technology exploits the use of leading and trailing edge control surfaces to aeroelastically shape the wing, with the resulting aerodynamic forces from the flexible wing becoming the primary means for generating control power. With AAW, the control surfaces then act mainly as tabs and not as the primary sources of control power as they do with a conventional control philosophy. As a result, wing flexibility is seen as an advantage rather than a detriment since the aircraft can be operated beyond reversal speeds and still generate the required control power for maneuvers. Figure 1 illustrates conceptually the differences between AAW technology and a conventional control approach.

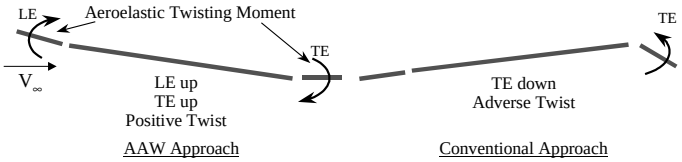

Figure 1 - AAW vs. Conventional Control

Wings designed with AAW technology are not subject to control surface effectiveness constraints, and thus have the potential to be lighter and/or more aerodynamically efficient. These more favorable aerodynamic characteristics may include higher aspect ratio and lower thickness ratio, trends normally associated with higher structural weight. It is likely that the wing geometry that takes maximum advantage of AAW will be different than the optimum wing geometry for a

---

* Graduate Research Assistant
† Assistant Professor, Aerospace Engineering
‡ Chief Engineer, Active Aeroelastic Wing Program
§ Senior Engineering Specialist

Presented at CEAS/ AIAA/ ICASE/ NASA Langley International Forum on Aeroelasticity and Structural Dynamics, Williamsburg, VA, June 22-25, 1999.

design with conventional control philosophy. Put in other terms, if AAW technology is simply applied to a wing geometry designed with current control technology, it is possible, and likely, that the benefits achieved will not be as high as for another wing designed explicitly with AAW technology in mind. In fact, Yurkovich confirmed this notion in a study where Taguchi methods were used to understand the relationship between wing weight and wing geometry for both an Active Flexible Wing (AFW, a.k.a. AAW) design and a conventional control design[5,6]. He showed that the maximum reduction in wing structural weight achieved by the use of AFW occurred at higher aspect ratios and lower thickness ratios. Conversely, he showed the minimum weight savings occurred at lower aspect ratios and higher thickness ratios, designs typical of current fighter technology[5]. Thus, AAW could produce a dramatic paradigm shift in wing design, allowing the use of wing geometries traditionally considered "poor" from a structural viewpoint, but "good" from an aerodynamic one.

For this paradigm shift in wing geometry design to occur, and the maximum potential of AAW technology to be realized, a clear comparison between AAW and a conventional control approach over the wing geometry design space must be provided to the conceptual level designer. This guidance, in part, will include the influence of wing design parameters (e.g., aspect ratio, taper ratio, etc.) on structural weight which can be expressed as equations to be used in the synthesis and sizing of a new fighter concept. Traditionally, these equations have been regressions of historical data, but since AAW is a new technology and falls outside the range of validity of the historical data, one must rely on physics-based simulation to generate these relations. This challenge of designing new aircraft concepts for which the historical database is invalid and more detailed simulations are required has been addressed in other arenas of aerospace systems design. References [7] and [8] used finite element methods and equivalent laminated plate analysis, respectively, in conjunction with a Design of Experiments/Response Surface Methodology (DOE/RSM) to generate wing weight response surface equations (RSE) as a function of wing geometry for a High Speed Civil Transport (HSCT) concept. In addition, Reference [9] demonstrated a procedure to develop wing bending material weight equations for a HSCT using finite element based structural optimization. The equations were obtained by a response surface methodology in which a quadratic polynomial was fit to data obtained from a set of structural optimizations. These equations were then incorporated into a synthesis/sizing code to replace the historically based equations being used in the code. The motivation for these studies was due to the fact that the HSCT has very few historical counterparts, thus making the weight equations in the synthesis/sizing code, which were primarily developed from a database of subsonic transports, highly questionable.

AAW technology faces a similar challenge. Traditional weight equations used in the sizing of fighter concepts will not likely provide accurate estimates of wing structural weight. Instead, detailed aerodynamic and structural simulations, incorporating accurate modeling of AAW technology, must be used to understand the new relationships between wing weight and wing geometry. It is to this end that this paper represents a first attempt.

Tools

Response Surface Methodology

This paper seeks to understand how wing design objectives, such as wing weight, vary with changes in wing geometry of a fighter concept and then attempt to quantify this variation in the form of equations which could be used by future conceptual designers in making wing geometry decisions. These equations are developed for a conventional control approach and an AAW approach, so that a clear comparison of the two control schemes can be made. To achieve this, the authors utilize DOE/RSM[10,11]. These techniques employ design of experiments and statistical multivariate regression to relate a response to a set of contributing variables, often when this relationship is either too complex or unknown to find analytically[12]. Such is the case with the relationship between wing weight and wing geometry. Thus, an empirical approach must be used to develop an approximate model of the exact relationship. The approximate model, for the purposes of this study, is a 2nd order polynomial equation, also referred to as a RSE, and takes the following form:

$$R = b_0 + \sum_{i=1}^{k} b_i x_i + \sum_{i=1}^{k} b_{ii} x_i^2 + \sum_{i=1}^{k-1} \sum_{j=i+1}^{k} b_{ij} x_i x_j \qquad (1)$$

The coefficients (b_i, b_{ii}, b_{ij}) are estimated using least squares regression of computer simulated data, which is provided in an organized manner through a DOE.

After checking the statistical and predictive accuracy of the RSE within the designated design space, the designer can use the RSE as a convenient model with which to examine a very complex design space. It is precisely this visibility that gives DOE/RSM an advantage over traditional optimization approaches, particularly in a conceptual design setting where design "openness" is desirable.

Parameterization of Finite Element and Aerodynamic Models

The wing weight is estimated for several wing geometries by means of the multidisciplinary optimization tool, Automated Structural Optimization System (ASTROS)[13]. ASTROS combines finite element methods with aerodynamic and trim modules, in conjunction with gradient-based optimization routines to optimize the thickness of structural members to minimum weight while meeting user-defined constraints, such as static and dynamic aeroelastic requirements. Particularly when using finite element methods, a change of external geometry can often prove to be a challenging and time-consuming task since a new model must be created, usually in a manual fashion. The authors have addressed this problem by assuming that the internal structural

layout (i.e., number of ribs and spars) remains unchanged from some baseline model. Thus, each finite element model (FEM) which corresponds to a geometry different than the baseline has the same number of nodes as the baseline model. The locations of these nodes are parametrically defined by the external wing geometry. In essence, the mesh is "pushed and stretched" from its baseline value, which means that the connectivity of each element will remain unchanged as long as the changes in geometry stay within certain limits. The location of most of the nodes are specified to remain at the same percentage of span and same percentage of chord length as the external geometry of the wing changes from its baseline geometry. The location of these nodes for the new geometry are given by the following relationships:

$$x_{new} = x_{lenew} + \left(\frac{x_{base} - x_{lebase}}{x_{tebase} - x_{lebase}} \right) * (x_{tenew} - x_{lenew}) \qquad (2)$$

$$y_{new} = \frac{y_{base}}{(b/2)_{base}} * (b/2)_{new} \qquad (3)$$

where the subscript *base* refers to the baseline geometry, the subscript *new* refers to the new geometry, x_{te} is the streamwise location of the wing trailing edge corresponding to the node of interest, similarly x_{le} is the streamwise location of the leading edge, and *(b/2)* is the aircraft semispan (see Figure 2 for the definition of the coordinate system).

However, not all of the model's nodes follow the rules of Equations 2 and 3. Notable exceptions include:

- Leading edge hingeline nodes – The rule that governs the location of these nodes ensures that each hinge remains perpendicular to the leading edge spar.
- Nodes near side-of-body – The spanwise location (y value) of side-of-body nodes remains fixed, since the width of the fuselage is assumed to remain constant for each model.
- Carry-thru structure nodes – These nodes define bar elements that must be perpendicular to the fuselage.
- Tip missile nodes – The location of these nodes are defined so that the shape of the missile remains the same, but moves to follow the wing tip of the new configuration.

Figure 2 identifies for the baseline model the above mentioned nodes whose locations are defined by rules different than Equations 2 and 3.

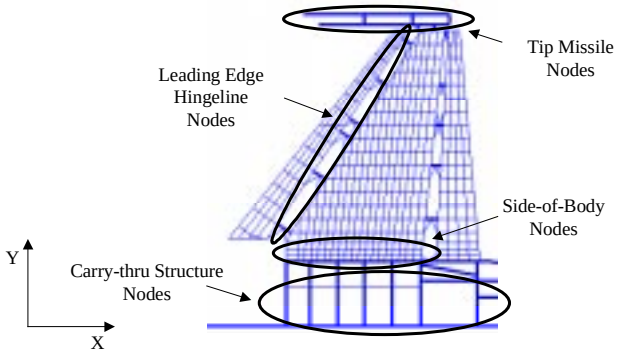

Figure 2 - Components of Finite Element Model

For a new geometry, the vertical location (z value) of each wing box node is calculated using Equation 4. Equation 4 is based on the premise that each node of the wing box has a "partner" node which shares the same x and y value, but whose vertical location differs depending on whether the node is on the upper or lower surface. In addition, Equation 4 assumes that the camber of the wing is small and that the mean camber line remains fixed for each geometry (where the mean camber line is defined by the midpoint between the upper and lower surface).

$$z_{new} = z_{meancamber} \pm (z_{base} - z_{meancamber}) * \frac{(t/c)_{new}}{(t/c)_{base}} \frac{(x_{tenew} - x_{lenew})}{(x_{tebase} - x_{lebase})} \qquad (4)$$

Since this study is exploring only the effect of wing geometry parameters on wing weight, the nodes associated with the vertical tail, horizontal tail, and fore- and aft- fuselage remain unmoved for each new model. In addition, the authors, in the interest of keeping the comparison of each geometry as "fair" as possible, have constrained the mean aerodynamic center to have the same x value for each model.

Along with changes in the node locations, there are other features of the FEM that require updates with changes in wing geometry. These include rotational springs that are used to transfer load from the control surfaces to the wing box. These springs are located at the control surface hingelines and whose stiffness' are dependent on the mean chord and area of its corresponding control surface as given by the following relationship:

$$k_{new} = k_{base} \left(\frac{c_{csnew}}{c_{csbase}} \right) \left(\frac{S_{csnew}}{S_{csbase}} \right) \text{ (lb-in/rad)} \qquad (5)$$

where k is spring stiffness, c_{cs} refers to the mean chord length of the control surface corresponding to the spring of interest and S_{cs} refers to the area of the same control surface.

Also, the control surface hingelines are defined by local coordinate systems so that rotations about the hingeline are expressed in terms of the surfaces' coordinate system as opposed to the global coordinate system. As a result, as the geometry of the wing changes, so too must the coordinate systems that define the direction of the hingelines. The update of the coordinate systems, the hingeline spring stiffness, and the parametric definition of the nodes is performed in a spreadsheet and imported to the ASTROS input file for each new geometry.

In addition to the structural model, an aerodynamic model (linear, 2-D) is also modified for a change in wing geometry. Similar to the structural model, the number of panels in the aerodynamic model remains the same from case to case, with their location being a function of the wing geometry. A spreadsheet application is also used to parameterize the aerodynamic model. The structural model (upper half) and the aerodynamic model (lower half) are shown in Figure 3 for two different wing geometries.

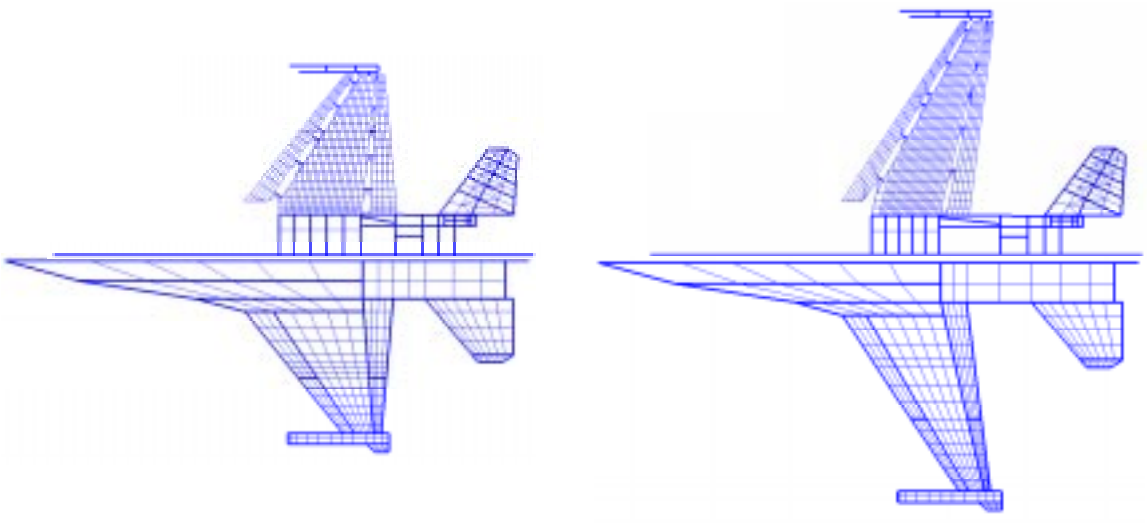

AR = 3.0, λ = 0.2 AR = 5.0, λ = 0.2

Figure 3 - Finite Element Models and Aerodynamic Models for Two Different Configurations

Modeling of AAW by Trim Optimization

The basic equation for static aeroelastic analysis by the finite element method is given by:

$$[[K]-q[A]]\{u\}+[M]\{\ddot{u}\}=[P]\{\delta\} \tag{6}$$

where [K] is the stiffness matrix, [A] is the aerodynamic influence matrix transformed to the structural degrees of freedom, [M] is the mass matrix, [P] is a matrix of the rigid aerodynamic force coefficients due to non-acceleration trim parameters, q is the dynamic pressure, and {δ} is the non-acceleration trim parameter values (e.g., aileron deflection, steady roll rate). For static aeroelastic trim, Equation 6 is reduced to the following equation, which in essence, is simply a balance of aeroelastic and inertial forces[14].

$$[L]\{\ddot{u}_r\}=[R]\{\delta\} \tag{7}$$

where [L] is the resultant aeroelastic mass, {$\ddot{u}_r$} is a vector of rigid body accelerations, and [R] is the resultant aeroelastic trim forces. In the case where the number of free trim parameters is equal to the number of supported degrees of freedom (DOF), Equation 7 has a closed form solution. For example, an antisymmetric rolling maneuver with a specified steady roll rate is a one DOF trim problem in which the negative moment about the aircraft centerline due to the roll rate must be balanced by the positive moment created by a control surface deflection. If only one control surface is used, then the calculation of the control surface rotation to trim the aircraft to the user-given roll rate is elementary. However, if multiple control surfaces (i.e., redundant surfaces) are desired to trim the aircraft to a steady state roll, then the closed form solution no longer exists. The trim solution must then be formulated as an iterative problem to determine the "best" combination of control surface rotations that trim the aircraft. Older versions of ASTROS have solved Equation 7 for non-redundant control surfaces, but a new module of ASTROS poses the solution of Equation 7 for redundant control surfaces as an optimization problem to minimize an objective of interest to the structural designer[15].

The trim optimization capability is of relevance to this study as AAW technology makes use of multiple, redundant control surfaces, and the authors desire to determine the optimal combination of control surface rotations for each maneuver to which the structure will be sized, which include both symmetric and antisymmetric maneuvers. In previous work, the objective of the trim optimization problem has been to minimize the overall control surface actuator command signal or in other terms, control energy[16,17]. As the ultimate goal of AAW technology is to reduce weight, the authors have formulated the trim optimization problem for the symmetric maneuvers as a minimization of root bending moment (RBM), subject to the trim balance requirement (satisfaction of Equation 7), control surface travel limits, and hinge moment (HM) constraints. Zillmer in Reference [18] also posed the trim optimization in a similar manner though using a composite function of stress, drag, and buckling load as the trim optimization objective. For the current case, the symmetric trim optimization problem can be formally stated as:

Minimize: RBM

Subject to: $-30^o \le \delta_{LEI} \le 5^o$, $-30^o \le \delta_{LEO} \le 5^o$,
$-30^o \le \delta_{TEI} \le 30^o$, $-30^o \le \delta_{TEO} \le 30^o$,
$-30^o \le \delta_{TAIL} \le 30^o$, $-10^o \le \alpha \le 30^o$
$-3.0*10^5 \le HM_{LEI} \le 3.0*10^5$,
$-1.0*10^5 \le HM_{LEO} \le 1.0*10^5$,
$-1.5*10^5 \le HM_{TEI} \le 1.5*10^5$,
$5.0*10^4 \le HM_{TEO} \le 5.0*10^4$ (lb-in)

$$[L]\{\ddot{u}_{trim}\} - [R]\{\delta_{trim}\} \le tolerance$$
$$[R]\{\delta_{trim}\} - [L]\{\ddot{u}_{trim}\} \le tolerance$$

Design Variables: α, δ_{LEI}, δ_{LEO}, δ_{TEI}, δ_{TEO}, δ_{TAIL}

where α is the angle of attack, δ are the control surface deflections, LEI refers to the inboard leading edge surface, LEO is the outboard leading edge surface, TEI corresponds to the inboard trailing edge surface, and TEO is the outboard trailing edge surface. By formulating the optimization problem in this manner, the authors hope to show that the wing control surfaces for the symmetric maneuvers can be used to tailor the load distribution and provide load relief at the wing root, thus ultimately reducing wing weight.

For the antisymmetric maneuvers, the trim optimization is formulated as a minimization of the total hinge moments, subject once again to the surface travel limits, hinge moment constraints, and trim balance requirements, as given formally by:

Minimize: $HM_{LEI} + HM_{LEO} + HM_{TEI} + HM_{TEO}$

Subject to: $-30^o \le \delta_{LEI} \le 5^o$, $-30^o \le \delta_{LEO} \le 5^o$,
$-30^o \le \delta_{TEI} \le 30^o$, $-30^o \le \delta_{TEO} \le 30^o$
$-3.0*10^5 \le HM_{LEI} \le 3.0*10^5$,
$-1.0*10^5 \le HM_{LEO} \le 1.0*10^5$,
$-1.5*10^5 \le HM_{TEI} \le 1.5*10^5$,
$5.0*10^4 \le HM_{TEO} \le 5.0*10^4$ (lb-in)

$$[L]\{\ddot{u}_{trim}\} - [R]\{\delta_{trim}\} \le tolerance$$
$$[R]\{\delta_{trim}\} - [L]\{\ddot{u}_{trim}\} \le tolerance$$

Trim Optimization Design Variables: δ_{LEI}, δ_{LEO}, δ_{TEI}, δ_{TEO}

Both of the trim optimization problems above are solved using a Modified Method of Feasible Directions algorithm within the commercial software MICRO-DOT[19]. Reference [15] discusses in detail the theory of the new ASTROS trim optimization module, and how the trim optimization module fits into the overall ASTROS framework.

It must be noted that the authors acknowledge that the trim optimization problem is not a trivial one, and that the selection of the best objective function is open to much research and debate.

Baseline Structural and Aerodynamic Models

Figure 4 shows the structural model for the baseline geometry. It is a preliminary design finite element model of a lightweight composite fighter aircraft with 4 wing control surfaces (2 trailing edge, 2 leading edge) and a horizontal tail[20,21]. It corresponds to a wing with an aspect ratio of 3.4, a total planform area of 330 ft^2, a taper ratio of 23.2%, a leading edge sweep of 37.0^o, and a thickness ratio of 4%. The skins of the wing are made up of 4 composite orientations, 0^o, $\pm 45^o$, and 90^o plies, where the thickness of the -45^o and $+45^o$ orientations are constrained to be equal. In addition, the composite wing skins are designed (*tailored*) in thickness and percentage of thickness to orientations, via ASTROS optimization routines, to meet specified maneuver and strength requirements[22].

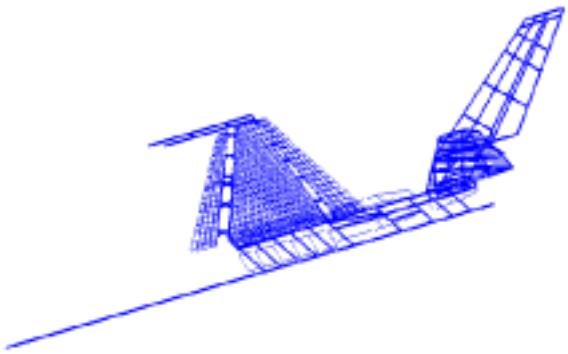

Figure 4 – Structural Model for Baseline Geometry

The aerodynamic model is shown in Figure 5. It is a flat panel Carmichael[23] model containing 143 vertical panels and 255 horizontal panels. It also contains paneling for the four wing control surfaces and horizontal tail to coincide with the control surfaces on the structural model. ASTROS has been modified to allow inclusion of Carmichael panel geometry and aerodynamic influence coefficients which then replace the existing aerodynamic database entities created by USSAERO, ASTROS' original aerodynamic module[15]. Carmichael aerodynamic influence coefficients are produced for two Mach numbers, 1.2 and 0.95, for both symmetric and antisymmetric conditions[22].

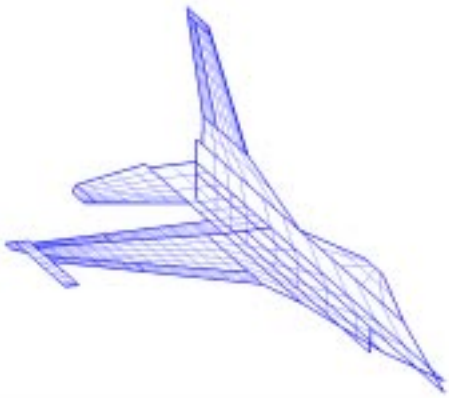

Figure 5 - Aerodynamic Model for Baseline Geometry

The design variables in the structural optimization are the layer thickness of the composite skins. The number of design variables is 78 due to physical linking of the skin elements. Internal structure and carry-thru structure remain fixed for this study. Table 1 shows the maneuver conditions and strength constraints to which the structure is designed.

Table 1 - Maneuver Conditions and Design Constraints

Maneuver Condition	Design Constraint
1) Mach 0.95, 10,000 ft. 9g Pull Up	fiber strain: 3000 με tension 2800 με compression
2) Mach 1.20, Sea Level -3g Push Over	fiber strain: 3000 με tension 2800 με compression
3) Mach 0.95, 10,000 ft. Steady State Roll = 180^{O}/s	fiber strain: 1000 με tension 900 με compression Outboard aileron effectiveness $\geq$ 0.142
4) Mach 1.20, Sea Level Steady State Roll = 100^{O}/s	fiber strain: 1000 με tension 900 με compression Rolling surface effectiveness $\geq$ 0.06

For the conventionally controlled models, the horizontal tail is used to trim the aircraft for both of the symmetric maneuvers, and the outboard aileron is used to trim the aircraft for the subsonic roll. For the supersonic roll a blending of inboard aileron and horizontal tail deflection is used, similar to the F-16, where the horizontal tail deflects 0.38^{o} antisymmetrically for every degree of inboard aileron deflection. For the AAW cases, all five control surfaces are used for the symmetric maneuvers, and only the four wing control surfaces are used for the rolling maneuvers. In addition, the surface effectiveness constraints are eliminated for the rolling maneuvers when using AAW technology, since as was suggested earlier, wings designed with AAW are not subject to surface effectiveness constraints.

Results

Design Space Definition

The first phase of the study is to define the wing geometry design variables of interest and their ranges (i.e., define the design space). The fighter concepts that this study is examining have trapezoidal wings. As a result, only four variables are needed to uniquely define the planform of the wing. The authors have assumed that the wing area of each configuration will remain constant, in addition to the sweep of the 40% chord line. Thus, there are two remaining planform parameters that can be varied. The authors have chosen aspect ratio and taper ratio as the planform variables, and thickness ratio as an additional design variable, since it so heavily influences wing torsional stiffness and thus, weight. Table 2 lists the variables and their associated ranges, which are based, in part, on the interests of the authors and also on the limitations of "stretching" the finite element mesh too far from its baseline value.

Table 2 – Wing Design Variables and Ranges

Design Variable	Symbol	Min. Value	Max. Value
Aspect Ratio	AR	3.0	5.0
Taper Ratio	λ	0.2	0.4
Thickness Ratio	t/c	0.03	0.06

Design of Experiments

Wing weight RSEs are created for both a conventional control philosophy and an AAW approach. These equations are determined by least square regression of weight results calculated at a finite set of points in the design space. The authors have chosen a face-centered central composite DOE[10] to provide the points at which wing weight will be found. Table 3 shows the DOE table for the three design variables, and the responses that are collected. A value of –1 for a design variable indicates that the variable is at its minimum

Table 3 - Design of Experiments Table

	AR	λ	t/c	$Weight_{Conv}$ (lb)	$Weight_{AAW}$ (lb)
Case 1	-1	-1	-1	401.90	334.60
Case 2	-1	-1	+1	182.70	126.00
Case 3	-1	+1	-1	466.10	407.30
Case 4	-1	+1	+1	199.60	161.20
Case 5	+1	-1	-1	1342.60	833.70
Case 6	+1	-1	+1	400.30	392.10
Case 7	+1	+1	-1	2086.30	1070.20
Case 8	+1	+1	+1	561.10	328.50
Case 9	-1	0	0	278.00	226.00
Case 10	+1	0	0	630.10	460.90
Case 11	0	-1	0	378.70	286.90
Case 12	0	+1	0	450.40	408.30
Case 13	0	0	-1	772.20	608.50
Case 14	0	0	+1	286.30	236.70
Case 15	0	0	0	410.50	380.50

value. Likewise, a value of +1 indicates the design variable is at its maximum, and a value of 0 refers to the mean of the design variable.

For each geometry, given by a row in the DOE table, wing weight is calculated by performing an ASTROS structural optimization for both a conventional control approach and an AAW approach ($Weight_{AAW}$, $Weight_{Conv}$). Wing weight here refers only to the weight of the wing box skins. The weight of internal structure, nonstructural mass, and the weight of the control surfaces is not considered, as the authors are more interested in the relative weight differences between AAW technology and a conventionally controlled design, rather than the absolute weight itself.

Calculation of Wing Weight

The estimation of the wing weight for the conventionally controlled designs is a relatively straight-forward process in which the skin thicknesses of the structural model are optimized to meet previously defined maneuver requirements (Table 1), where the maneuvers are performed using standard control surfaces. The final weights for each case are shown in Table 3 ($Weight_{Conv}$). For the AAW cases, the process is not so simple, as multiple control surfaces are used and whose settings are dependent on results of a trim optimization. Originally, the intent was for the trim optimization process to be performed within the structural optimization loop[15], as the optimal control surface deflections are a function of the structural design. In other words, for each iteration in the structural optimization, the control surface deflections for the current structural design would be optimized according to the formulation described earlier. Then, with these new deflections the structural optimizer would proceed to take another step, pause again for trim optimization, and so on, until the structural optimization objective, wing weight, converged. However, difficulty in implementing the software mandated that the trim optimization be done separately from the structural optimization. Instead, trim optimization is performed only on the starting structural design (i.e. those laminate thicknesses which describe the starting point of the structural optimization). This, clearly, is a limitation as the optimal surface deflections for the starting structural design will not be optimal for the final structural design.

The results of the trim optimization, then, are control surface deflections for each of the maneuvers to which the structure is sized, with the exception of the supersonic symmetric maneuver (Maneuver 2). The authors decided not to perform trim optimization on the supersonic push over maneuver, because during the optimization of the conventional cases, the constraints associated with this maneuver were never active. In essence, Maneuver 2 contributed little, if nothing, to the sizing of the structure, and thus the authors, being limited in time, decided that this maneuver could be neglected in the trim optimization procedure. As a result, even for the AAW cases only the horizontal tail was used to trim the aircraft in Maneuver 2. Table 4 shows the final deflections from the trim optimization for each case of the DOE table. The columns refer to the DOE case numbers, and the rows correspond to the optimal control surface deflections (and angle of attack) for each maneuver. All units are in degrees, and a positive deflection of the leading edge surface is nose-up, and a positive deflection of the trailing edge surfaces and horizontal tail is tail-down. Also, due to difficulties with running Case 6, the authors decided to use the optimal deflections of Case 5 for Case 6.

Notice that consistently, for all cases, the trim optimizer drove the outboard leading and trailing edge surfaces to large negative values for the symmetric pull up (Maneuver 1). As a result, more load is shifted inboard, or in other words, the center of pressure moves inboard, thus causing a significant reduction in root bending moment. For the subsonic rolling maneuver (Maneuver 3), the optimizer tended to favor usage of the trailing edge surfaces, which makes sense, as these surfaces are far more effective in roll than the leading edge surfaces at subsonic speeds. Notable exceptions to this trend, though, include Cases 5, 6, 7, 8, and 10 where one sees that some leading edge deflection is needed. These cases correspond to aspect ratio 5 wings, where even at subsonic speeds, the trailing edge surfaces are beginning to lose effectiveness. For Maneuver 4, the optimizer relied heavily on the leading edge surfaces and very little on the trailing edge.

Table 4 - Final Control Surface Rotations for each Trim Optimization

		1	2	3	4	5	6	7	8	9	10	11	12	13	14	15
Maneuver 1	α	13.0	13.7	12.2	12.8	9.3	9.3	8.7	10.0	12.2	9.8	11.6	10.5	10.2	11.1	10.8
	δ_{TAIL}	1.9	2.9	1.7	1.9	-1.7	-1.7	-1.0	0.0	-1.8	-0.1	-0.3	1.5	1.4	2.5	2.3
	δ_{TEI}	-2.1	-2.1	0.0	0.0	0.0	0.0	0.0	0.0	0.0	0.0	0.0	0.0	0.0	-0.6	0.0
	δ_{TEO}	-30.0	-30.0	-25.6	-24.9	-29.9	-29.9	-30.0	-27.6	-15.1	-30.0	-30.0	-25.9	-30.0	-29.0	-29.8
	δ_{LEI}	-16.8	-16.8	-18.6	-21.6	0.0	0.0	0.0	0.0	-17.8	0.0	-17.0	0.0	0.0	0.0	0.0
	δ_{LEO}	-30.0	-30.0	-30.0	-30.0	-30.0	-30.0	-30.0	-30.0	-30.0	-30.0	-30.0	-30.0	-30.0	-30.0	-30.0
Man. 3	δ_{LEI}	0.0	0.0	0.0	0.0	0.0	0.0	5.0	5.0	0.0	5.0	0.0	0.0	0.0	0.0	0.0
	δ_{LEO}	0.0	0.0	0.0	0.0	5.0	5.0	5.0	5.0	0.0	5.0	0.0	0.0	0.0	0.0	0.0
	δ_{TEI}	-1.2	-1.1	-3.5	-3.8	-2.8	-2.8	30.0	10.9	-1.7	0.0	-1.4	-13.1	-6.1	-4.2	-4.7
	δ_{TEO}	9.5	7.8	10.7	8.9	23.4	23.4	23.7	11.1	8.6	13.8	11.4	13.6	16.8	11.1	12.3
Man. 4	δ_{LEI}	2.8	5.0	5.0	1.6	3.2	3.2	1.7	4.5	0.3	3.3	2.3	2.2	0.7	0.6	1.9
	δ_{LEO}	5.0	5.0	0.3	1.2	-6.7	-6.7	0.0	0.0	5.0	0.0	5.0	4.4	5.0	5.0	4.9
	δ_{TEI}	0.3	0.8	1.6	0.1	0.0	0.0	0.0	0.0	0.0	0.1	0.5	0.0	0.0	0.0	1.3
	δ_{TEO}	1.6	3.6	1.8	8.0	0.6	0.6	0.6	1.1	7.2	1.0	1.4	1.4	1.3	8.9	2.2

This is consistent with the AAW claim that when trailing edge surfaces are reversing, the leading edge surfaces can be used to provide roll control. It is interesting to note, though, that for the high aspect ratio cases (5, 6, 7, 8, and 10), the optimizer drove the inboard leading edge surface to positive deflection, but left the outboard leading edge at zero deflection (and for Case 5, even drove it to negative deflection). For these cases the inboard surface is much more effective than the outboard surface. In considering that the wing is flexible, one can envision that a positive deflection of the inboard leading edge surface torques the wing in a positive manner so that even the outboard portion of the wing is twisting to provide positive roll moment. As a result, the optimizer uses more of the inboard leading edge surface.

Once the trim optimization is complete, the optimal deflections are carried over to the structural optimization by the following procedure:

1) In the structural optimization for the symmetric maneuver, the wing control surfaces (δ_{LEI}, δ_{LEO}, δ_{TEI}, δ_{TEO}) are set to their optimized values, and the angle of attack and horizontal tail deflection are the free trim parameters.
2) In the structural optimization for Maneuver 3, a new surface is created that links all four wing surfaces together according to gear ratios that dictate how much the control surfaces deflect with respect to the new surface. This new surface is defined by a CONLINK entry in the ASTROS bulk data. These gear ratios are calculated by dividing the optimal deflections of each of the wing surfaces by the optimal deflection of the outboard trailing edge surface. For example, for the first case the gear ratios are 0.0, 0.0, -0.126, and 1.0 corresponding to LEI, LEO, TEI, and TEO, respectively. This new "artificial" surface then becomes the free trim parameter for the rolling maneuver, and the gear ratios remain fixed through the course of the structural optimization.
3) In the structural optimization for Maneuver 4, another new surface is created similar to in Maneuver 3 with the one difference that the gear ratios are calculated by dividing by the optimal deflection of the outboard leading edge surface. As a result, the gear ratios for the first case would be 0.56, 1.0, 0.06, and 0.32. For Cases 7, 8, and 10, where the optimal deflection of the outboard leading edge is zero, the inboard leading edges surface is used as the basis.

Gear ratios are not created for the symmetric maneuver, because the authors discovered that if the wing surfaces were geared to the horizontal tail, then as the structural optimization progressed these surfaces would deflect to unreasonably large values, because they were "slaved" to the horizontal tail. This was particularly true for those surfaces whose optimal values were already at the limit of their allowable deflection (e.g., in Case 1, δ_{LEO} from Maneuver 1). As a result, the authors decided to fix the wing surfaces to their optimal values, let them remain fixed through the structural optimization and let angle of attack and horizontal tail rotation be the free trim parameters.

Regression of Data to Create RSEs

After the optimized structural weights are calculated for each case of the DOE table ($Weight_{Conv}$ and $Weight_{AAW}$), least squares regression is performed on both responses to create quadratic RSEs (Equation 1) of weight as a function of wing geometry. The regression is performed with the aid of the statistical software package, JMP[24], which also provides valuable statistical information about the fit of the RSE to the data that was used to create it. Among the important pieces of information pertaining to the fit of the RSE is the R^2 value. In essence, the R^2 measures how much of the variation in the data is being captured by the assumed quadratic model. An R^2 of 1 indicates that all variation in the data is being captured by the model, or in other words the quadratic model perfectly fits the data. Lower R^2 values indicate that not all of the variation in the data is being captured. For the conventional approach weight, the R^2 value turned out to be mediocre, at best, at a value of 0.85, while the AAW weight R^2 value was a little better at 0.92. This prompted the authors to explore the possibility of transforming the response in an attempt to improve RSE fit without the need to run any more additional cases. This transformation is known as a power transformation and is discussed in detail in Reference [25]. The theory of this transformation is beyond the scope of this paper, but its steps are outlined here:

1) Raise the response ($Weight_{Conv}$ and $Weight_{AAW}$) for each case of the DOE table to a power Λ, where Λ is determined by the Method of Maximum Likelihood[25]. This results in a new transformed response, w ($w=Weight^{\Lambda}$).
2) Perform least square regression on the transformed response, w, to create a quadratic RSE for the new response.
3) Then, to get the equation in terms of the original response, Weight, raise the RSE of w to the inverse of the power, Λ ($Weight = w^{1/\Lambda}$)

For the conventional control weight the best Λ is –0.8, while for the AAW weight the best transformation is the natural log transformation. A natural log transformation corresponds to a Λ of 0, which seems unintuitive since any response raised to 0 is 1. However, Reference [25] explains this reasoning by an expansion of Y^{Λ} and taking its limits as Λ goes to 0. The transformations result in the following RSEs for $Weight_{Conv}$ and $Weight_{AAW}$.

$$Weight_{Conv} = \begin{pmatrix} 0.00032\times AR^2 - 0.00025\times \lambda^2 - 1.053\times (t/c)^2 \\ -0.0034\times AR + 0.0031\times \lambda + 0.49\times (t/c) \\ -0.00114\times AR\times \lambda - 0.043\times AR\times (t/c) \\ -0.097\times \lambda\times (t/c) + 0.00607 \end{pmatrix}^{-1.25} \quad (8)$$

$$Weight_{AAW} = \exp\begin{pmatrix} -0.091\times AR^2 - 3.19\times\lambda^2 + 317.4\times(t/c)^2 \\ +1.27\times AR + 1.94\times\lambda - 49.1\times(t/c) \\ +0.20\times AR\times\lambda - 4.68\times AR\times(t/c) \\ +12.7\times\lambda\times(t/c) + 3.97 \end{pmatrix} \quad (9)$$

After the transformation, the R^2 values for the new weight equations improved considerably, with $Weight_{Conv}$ having an R^2 of 0.99 and $Weight_{AAW}$, a value of 0.98. Unfortunately, though, as a result of the transformation, the coefficients of each equation cannot be compared on a one-to-one basis as the equations are no longer pure quadratics. This is, indeed, one disadvantage of the power transformation. A gain in R^2 results in a loss of equation comparability. Equations 8 and 9 are graphed in Figures 6, 7, and 8 to provide a visual comparison of the weight equations for the two control approaches.

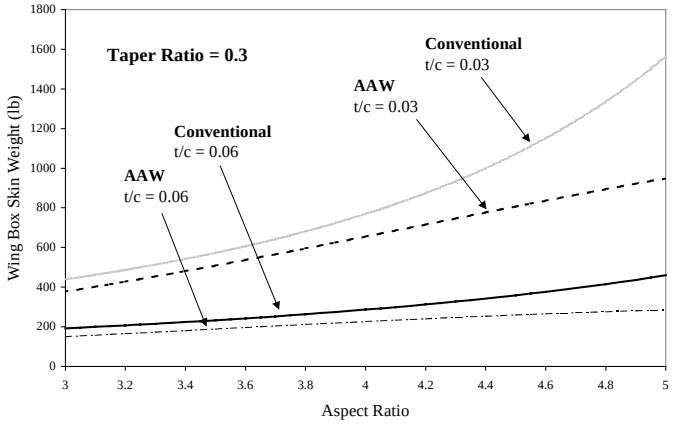

Figure 6 - Wing Weight vs. Aspect Ratio

Figure 6 is a plot of wing weight versus aspect ratio. One clearly sees the significant weight savings that AAW technology can provide particularly for the high aspect ratio, high thickness ratio cases. In addition, for the same weight AAW technology would allow the use of a higher aspect ratio wing, which agrees with the initial AAW claim that for the same amount of wing weight a better aerodynamically performing wing can be used.

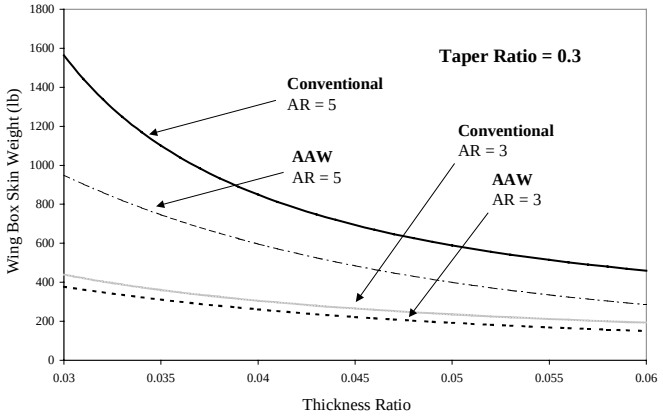

Figure 7 - Wing Weight vs. Thickness Ratio

Figure 7, which is a plot of weight versus thickness ratio, shows once again that maximum weight savings due to AAW technology occurs for the higher weight wings. This conclusion is similar to one made by Yurkovich in Reference [5]. In addition, one observes the significant impact that thickness ratio has on weight as weight decreases dramatically with increasing thickness ratio. It is important to note, however, that the weight equations do not consider the impact of drag, so it is reasonable to expect that at some higher thickness ratio, the weight would begin to rise. Also, one can begin to see why a quadratic model was a poor predictor of the exact relationship between weight and geometry, particularly for the conventional approach, as weight grows very quickly with decreasing thickness ratio.

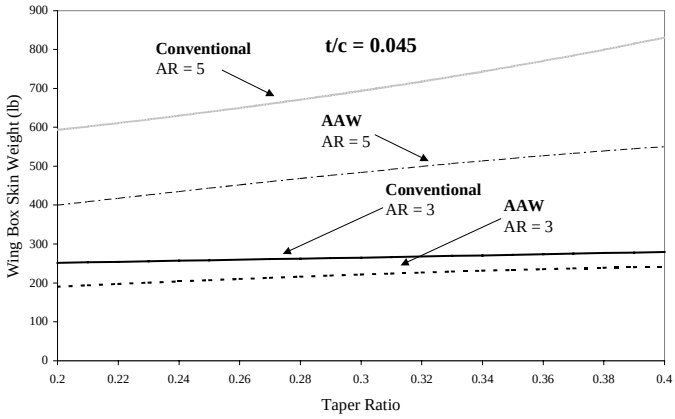

Figure 8 - Wing Weight vs. Taper Ratio

In the plot of weight versus taper ratio (Figure 8), one observes that taper ratio does not have nearly the impact on weight as do the other two geometry parameters. There is, though, the consistent trend of increasing weight with increasing taper ratio, which makes sense as more wing area (and thus more load) is shifted outboard as the taper ratio increases.

Validation

One final test of RSE fit is a validation test, where the wing weight is evaluated at a number of random points in the design space and compared to its value as predicted by the RSE. The conventional approach RSE is validated in Table 5 by evaluating the wing weight for four cases where each case corresponds to a random point in the wing geometry design space (Table 2). The weight from each case is then compared to that predicted by the RSE and a percent difference calculated.

Table 5 - Validation Results

Case #	$Weight_{Conv}$(Actual)	$Weight_{Conv}$(RSE)	Error
1	315.60	324.46	-2.81 %
2	422.40	408.70	3.24 %
3	333.40	356.21	-6.84 %
4	364.80	370.24	-1.49 %

Table 5 shows that the largest difference between the actual and RSE predicted weights is just under 7%, indicating that the RSE is a good predictor of the exact relationship between wing weight and wing geometry for the conventional approach. At the present time, a validation test has not been performed on the wing weight equation for AAW technology.

Conclusions

A process has been implemented by which wing weight equations are developed for a lightweight composite fighter considering both AAW technology and conventional control technology. For future design studies of advanced fighters that employ AAW technology, these equations could then be used to complement the historically based equations that are currently residing in standard synthesis/sizing codes. The keys of this wing weight generation process include the parameterization of preliminary design level models, design of experiments/response surface methodology techniques, and recent advances in aeroelastic design methods to include trim optimization for the modeling of AAW technology. Such a process is necessary to effectively design for some advanced technologies such as AAW where the historically based equations are no longer valid.

The study results indicate that AAW technology is an enabler for dramatically expanding the wing planform design space, allowing the use of better aerodynamically performing wings at significantly less weight penalty. AAW technology offers a solution to static aeroelastic design constraints, such as aileron effectiveness for rolling maneuvers, typically applied in aircraft design. In addition, the study showed that AAW technology can also provide root bending moment relief for symmetric maneuvers. Since this study did not include flutter constraints on the design, the benefits shown would be attributed to "advanced AAW", which would include a flutter suppression capability. Separation of these benefits will be a motivation for further work in this area. Additionally, the total impact of AAW technology on the vehicle system design has not been addressed here, but will also be addressed in future efforts.

Acknowledgments

This research was funded, in part, by a summer internship for Mr. Zink at Air Force Research Laboratories in Dayton, Ohio, under the supervision of Dr. Vipperla Venkayya.

References

1) Bisplinghoff, R.L., Ashley, H., and Halfman, R.L., Aeroelasticity, Dover Publications, Inc., Mineola, New York, 1955.

2) Miller, G.D., "Active Flexible Wing (AFW) Technology," Air Force Wright Aeronautical Laboratories, TR-87-3096, February 1988.

3) Perry III, B., Cole, S.R., and Miller, G.D., "A Summary of an AFW Program," Journal of Aircraft, Vol. 32, No. 1.

4) Pendleton, E., Griffin, K., Kehoe, M., and Perry, B., "A Flight Research Program for Active Aeroelastic Wing Technology," 37th AIAA/ASME/ASCE/AHS/ASC Structures, Structural Dynamics, and Materials Conference, April 1996.

5) Yurkovich, R., "Optimum Wing Shape for an Active Flexible Wing," 36th AIAA/ASME/ASCE/AHS/ASC Structures, Structural Dynamics, and Materials Conference, April 1995, AIAA-95-1220.

6) Yurkovich, R., "The Use of Taguchi Techniques with the ASTROS Code for Optimum Wing Structural Design," 35th AIAA/ASME/ASCE/AHS/ASC Structures, Structural Dynamics, and Materials Conference, April 1994, AIAA-94-1484.

7) DeLaurentis, D.A., Zink, P.S., Mavris, D.N., Cesnik, C.E.S., and Schrage, D.P., "New Approaches to Multidisciplinary Synthesis: An Aero-Structures-Control Application Using Statistical Techniques," 1996 World Aviation Congress, Los Angeles, CA, October 1996.

8) Mavris, D.M., and Hayden, W.T., "Probabilistic Analysis of an HSCT Modeled with an Equivalent Laminated Plate Wing," 1997 World Aviation Congress, Anaheim, CA, October 1997.

9) Kaufman, M., Balabanov, V., et. al., "Variable-Complexity Response Surface Approximations for Wing Structural Weight in HSCT Design," 34th Aerospace Sciences Meeting, Reno, NV, January 1996, AIAA-96-0089.

10) Myers, R.H., and Montgomery, D.C., Response Surface Methodology: Process and Product Optimization using

Designed Experiments, John Wiley & Sons, Inc., New York, 1995.

11) Li, G., Wang, H., Aryasomayajula, S.R., and Grandhi, R.V., "A Two-Level Optimization Approach for the Conceptual and Preliminary Design of Airframe Structures," 7th AIAA/USAF/NASA/ISSMO Symposium on Multidisciplinary Analysis and Optimization, St. Louis, MO, September 1998, AIAA Paper 98-4888.

12) DeLaurentis, D., Mavris, D.N., and Schrage, D.P., "System Synthesis in Preliminary Aircraft Design using Statistical Methods," 20th Congress of the International Council of the Aeronautical Sciences, Sorrento, Italy, September 1996.

13) Neill, D.J., Johnson, E.H., and Canfield, R., "ASTROS-A Multidisciplinary Automated Design Tool," Journal of Aircraft, Vol. 27, No. 12, 1990, pp. 1021-1027.

14) Johnson, E.H., and Venkayya, V.B., ASTROS Theoretical Manual, AFWAL-TR-88-3028, December 1988.

15) Love, M.H., Barker, D.K., Egle, D.D., Neill, D.J., and Kolonay, R.M., "Enhanced Maneuver Airloads Simulation for the Automated Structural Optimization System – ASTROS," 38th AIAA/ASME/ASCE/AHS/ ASC Structures, Structural Dynamics, and Materials Conference, April 1997.

16) Anderson, G., Forster, E., Kolonay, R., and Eastep, F., "Multiple Control Surface Utilization in Active Aeroelastic Wing Technology," Journal of Aircraft, Vol. 34, No. 4, 1997, pp. 552-557.

17) Volk, J. and Ausman, J., "Integration of a Generic Flight Control System into ASTROS," 36th AIAA/ASME/ASCE/AHS/ASC Structures, Structural Dynamics, and Materials Conference, April 1996, AIAA-96-1335.

18) Zillmer, S., "Integrated Multidisciplinary Optimization for Active Aeroelastic Wing Design," Air Force Wright Aeronautical Laboratories, WL-TR-97-3087, August 1997.

19) MICRO-DOT User's Manual, Version 1.0, Engineering Design Optimization, Inc., Santa Barbara, California, 1985.

20) Karpel, M., Moulin, B., and Love, M.H., "Modal-Based Structural Optimization with Static Aeroelastic and Stress Constraints," Journal of Aircraft, Vol. 34, No. 3, 1997, pp.433-440.

21) Zink, P.S., Mavris, D.N., Love, M.H., and Karpel, M., "Robust Design for Aeroelastically Tailored/Active Aeroelastic Wing," 7th AIAA/USAF/NASA/ISSMO Symposium on Multidisciplinary Analysis and Optimization, St. Louis, MO, September 2-4, 1998, AIAA-98-4781.

22) Barker, D.K. and Love, M.H., "An ASTROS Application with Path Dependent Results," AIAA/USAF/ NASA/ISSMO Multidisciplinary Analysis and Optimization Conference, Bellevue, WA, September 1996.

23) Carmichael, R.L., Castellano, C.R., and Chen, C.F., The Use of Finite Element Methods for Predicting the Aerodynamics of Wing-Body Combinations, NASA SP-228, October 1969.

24) SAS Institute Inc., JMP Computer Program and User's Manual, Cary, NC, 1994.

25) Box, G.E.P, and Draper, N.R., Empirical Model-Building and Response Surfaces, John Wiley & Sons, Inc., New York, 1987.